Anomalous luminescence of Eu^{2+} and Yb^{2+} in inorganic compounds

2003 J. Phys.: Condens. Matter 15 2645

(http://iopscience.iop.org/0953-8984/15/17/318)

INSTITUTE OF PHYSICS PUBLISHING JOURNAL OF PHYSICS: CONDENSED MATTER

J. Phys.: Condens. Matter **15** (2003) 2645–2665 PII: S0953-8984(03)59379-1

Anomalous luminescence of Eu^{2+} and Yb^{2+} in inorganic compounds

P Dorenbos

Interfaculty Reactor Institute, Delft University of Technology, Mekelweg 15, 2629 JB Delft, The Netherlands

E-mail: dorenbos@iri.tudelft.nl

Received 10 February 2003
Published 22 April 2003
Online at stacks.iop.org/JPhysCM/15/2645

Abstract

In many compounds the broadband emission of Eu^{2+} and Yb^{2+} is subject to a very large (0.6–1.2 eV) Stokes shift and it behaves peculiarly with temperature change. Conduction band states of the host compound are involved in this 'anomalous' emission. Cases of anomalous emission are identified and the conditions for it to occur studied. Clear trends with the size of the lanthanide ion, the size of the site occupied, the size of anions in the compound, and the binding strength of oxygen ligands were found. The trends are interpreted by models involving the Madelung potential and Pauling repulsion at the lanthanide site together with the Coulomb and isotropic exchange interactions within the lanthanide ion. The results provide information on the approximate location of the lowest $4f^{n-1}5d$ level relative to the bottom of the conduction band. The systematic variation with type of lanthanide and host lattice is discussed. Combining the results with information on the systematic variation in the fd transition energies, all energy levels for each divalent lanthanide can be approximately positioned relative to the conduction and valence band.

1. Introduction

After exciting a lanthanide ion from the $4f^n$ ground state to the $4f^{n-1}5d$ configuration, the system relaxes to the lowest fd state. From here a dipole-allowed radiative transition to lower $4f^n$ levels may take place, yielding broadband (FWHM 0.1–0.4 eV) emissions characterized by a Stokes shift of typically 0.1–0.5 eV [1, 2].

In most lanthanides, df emission is not observed. It may be thermally quenched at room temperature by means of intersystem crossing from the $4f^{n-1}5d$ configuration to the $4f^n$ configuration. This situation is commonly described by a configuration coordinate diagram [3]. In Sm^{3+}, Eu^{3+}, Tb^{3+}, Dy^{3+}, and Ho^{3+}, df emission is quenched because of rapid multiphonon relaxation from the lowest $4f^{n-1}5d$ state to lower-lying $4f^n$ levels. For the divalent lanthanides,

df emission has been observed for Sm^{2+}, Eu^{2+}, Tm^{2+}, and Yb^{2+}. In the other divalent lanthanides, again relaxation to lower-lying $4f^n$ levels quenches the df emission.

Another quenching mechanism was noticed for BaF_2:Eu^{2+} and CaF_2:Yb^{2+} where a strongly red-shifted broadband luminescence is observed that is different in character from the normal df emission [4]. Kaplyanskii and Feofilov [4] suggested an involvement of 6s states and later Reut [5] proposed that it is caused by a transition from a charge transfer state to the $4f^n$ ground state of the lanthanide ion. Subsequent studies demonstrate a complex structure of the emitting CaF_2:Yb^{2+} state, and a distortion due to the Jahn–Teller effect was suggested [6–8].

The matter was further resolved after the photoconductivity studies by Pedrini and co-workers [9, 10]. Their work provided the location of the energy levels of the divalent lanthanides in CaF_2, SrF_2, and BaF_2 relative to the conduction band states of the host crystal. On the basis of this, McClure and Pedrini [11] demonstrated a direct relationship between the presence of anomalous emission and the location of the excited 5d level inside or close to the conduction band of the host crystal. Applying this to SrF_2:Yb^{2+}, they showed that excitation to the 5d level leads to autoionization. The electron delocalizes over the surrounding Sr^{2+} cations and a trapped exciton-like state near the Yb^{3+} impurity is formed. The 'anomalous' emission is the radiative return to the ground state of Yb^{2+} which in essence is a metal-to-metal charge transfer (MMCT) as was originally proposed by Reut [5]. Subsequent studies by Moine *et al* [12, 13] on BaF_2:Eu^{2+} and Yb^{2+} in CaF_2, SrF_2, and BaF_2 further confirmed this impurity-trapped exciton model. Since then this trapping has been identified in various other Eu^{2+} and Yb^{2+}-doped compounds [14–20].

It is now accepted that the location of the 5d levels relative to conduction band states and the presence of 'anomalous' emission are related to each other. The precise location of the 5d levels is of importance in many areas of applied physics. For example, the thermal quenching of df emission and also ff emission is often caused by autoionization processes due to the proximity of conduction band states [17, 21]. Autoionization may lead to charge trapping phenomena which are beneficial in information storage phosphors for x-ray imaging and radiation dosimetry applications, but it may also lead to unwanted afterglow phenomena in scintillator applications [22, 23]. Energy losses in laser crystals are often caused by excited state absorption leading to autoionization [24]. Also the ability of lanthanides to trap a hole from the valence band or an electron from the conduction band is related to the location of energy levels relative to host levels. Despite its importance, surprisingly little is known on the location of 5d levels relative to the conduction band.

In this work, information on 'anomalous' emission of the divalent lanthanides is collected, and the systematic variation with the type of lanthanide ion and the type of host compound is studied. For example, anomalous emission is more frequently observed for the divalent lanthanides on large lattice sites like that of Ba^{2+} than on small sites like that of Ca^{2+}. The probability of anomalous emission also increases with decreasing size of the lanthanide ion, and it is more frequently observed for Yb^{2+} than for Eu^{2+}. Several interactions will be discussed in an effort to explain the trends found. These are:

(1) the changing Madelung potential and Pauling repulsion at the lanthanide site due to lattice relaxation around the lanthanide ion;
(2) the Coulomb attraction between the 5d electron and the lanthanide; and
(3) the isotropic exchange interaction between the 5d electron spin and the total spin of the $4f^{n-1}$ electrons.

The interactions combined yield a systematic variation of the 5d electron binding energy through the lanthanide series in accord with the trends found. Combining the results with the

known systematic variation in the fd transition energies [2], one may position the energy of the ground state and excited states for each divalent lanthanide relative to the top of the valence band and bottom of the conduction band of the host lattice.

2. Normal and anomalous emission in the divalent lanthanides

Figure 1 shows the $4f^n$ energy levels of the free divalent lanthanides. The energy difference $E(n, 2+, A)$ between the lowest $4f^n$ level at zero energy and the lowest $4f^{n-1}5d$ level of the divalent lanthanide ions in a compound behaves as [2, 25]

$$E(n, 2+, A) = E_{A\,\mathrm{free}}(n, 2+) - D(2+, A) - [\Delta S(2+, A)]. \tag{1}$$

Here, generalized notation is used where n is the number of electrons in the 4f shell of the $4f^n5d^0$ configuration, 2+ indicates the ionic charge of the lanthanide, and A indicates the type of compound. $E_{A\,\mathrm{free}}(n, 2+)$ is for each lanthanide ion a constant with a value close to the transition energy in the free divalent lanthanide ion. The solid curve in figure 1 connects $E_{A\,\mathrm{free}}(n, 2+)$ for La^{2+} ($n = 1$) up to Yb^{2+} ($n = 14$). One may simply shift this curve downward by the red-shift $D(2+, A)$ to obtain the fd absorption energy $E_{\mathrm{abs}}(n, 2+, A)$ for each lanthanide. A further shift by the Stokes shift $\Delta S(2+, A)$ provides the emission energies $E_{\mathrm{em}}(n, 2+, A)$. Values for $D(2+, A)$ and $\Delta S(2+, A)$ for more than 300 different compounds are available [25].

df emission in the divalent lanthanides is usually quenched by multiphonon relaxation from the 5d level to levels of the $4f^n$ configuration. There are a few exceptions. When the red-shift and Stokes shift place the 5d level of Sm^{2+} near to or below the $^5D_0$ state—see figure 1—df emission may occur. The same applies for Eu^{2+} when the level is shifted to near to or below $^6P_{7/2}$. When for Tm^{2+} the 5d level is not shifted too far towards the $^2F_{5/2}$ level, df emission can also be observed in Tm^{2+}. Finally, for Yb^{2+} there is no multiphonon relaxation path and df emission cannot be quenched in that way.

Figure 2 illustrates different emission mechanisms with a configuration coordinate diagram. To draw the diagram, realistic values from BaF_2:Eu^{2+} and SrF_2:Yb^{2+} data were used. Initially the system is in the $4f^n$ ground state, indicated by point A on parabola a. After excitation to the 5d level, which requires about 3.2 eV, point B on parabola b is reached. Subsequent lattice relaxation brings the system to point C and several routes can be followed from here. In the case of SrF_2:Yb^{2+}, the system relaxes to the impurity-trapped exciton state indicated by point E on parabola d. From here anomalous emission (arrow EF) takes place. It is characterized by a 0.6 eV wide (FWHM) and 1.55 eV high Stokes-shifted emission band. In the case of BaF_2:Eu^{2+} at room temperature, the system relaxes to point G on parabola e; this is followed by anomalous emission (arrow GF) at 590 nm. At low temperature, however, normal df emission at 403 nm (arrow CD) with a small Stokes shift of 0.17 eV has been reported for BaF_2:Eu^{2+} [25, 26].

Parabola c represents an excited state of the $4f^n$ configuration. Via the crossing point with parabola d, the anomalous emission is quenched and the excited $4f^n$ state becomes populated. The existence of the $^7F_6$ and $^2F_{5/2}$ levels in Sm^{2+} and Tm^{2+} is very likely the reason that anomalous emission has never been observed for these lanthanides. It has only been observed for Eu^{2+} and Yb^{2+}, precisely those lanthanides where excited $4f^n$ levels, that may quench anomalous emission, are absent.

Figure 3 illustrates a possible configuration of the lanthanide-trapped exciton in an MX_2 alkaline-earth halide compound. After fd excitation, the occupied 5d level is located just below the conduction band CB as illustrated in figure 3(a). It corresponds to point B in figure 2. Autoionization of the 5d electron to the conduction band leaves the lanthanide

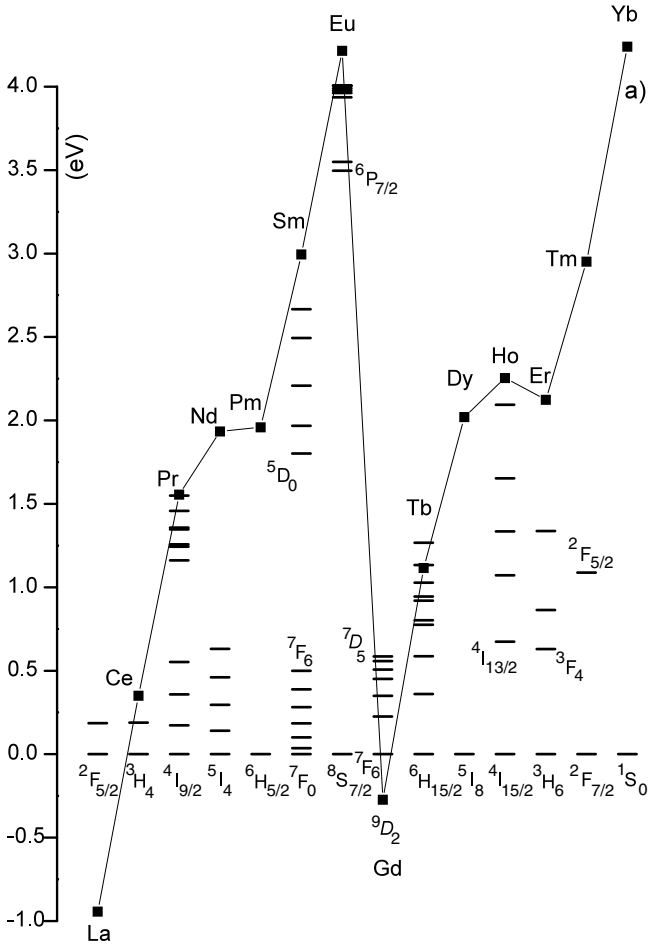

Figure 1. The energy level scheme of the free divalent lanthanides. The solid curve (a) connects the locations of the first $4f^{n-1}5d$ level.

ion in the trivalent state which has an about 19 pm smaller ionic radius; see figure 8. The neighbouring anions will relax towards Ln^{3+} as shown in figures 3(b) and (c). The Madelung potential at the lanthanide site becomes more negative and the (unoccupied) 5d levels of the lanthanide will move upward. The conduction band levels of the neighbouring M^{2+} cation probably move downward as illustrated in figure 3(d). The Coulomb attraction between the electron and the Ln^{3+} ion, together with the possible reduced Madelung potential at the nearby M^{2+} sites, localizes the electron in the lanthanide-trapped exciton configuration as illustrated in figure 3(e). This corresponds to point E in figure 2.

2.1. Anomalous Eu^{2+} emission

Identifying anomalous Eu^{2+} emission will be based on the following three aspects. (1) An abnormally large Stokes shift and width (FWHM) of the emission band. (2) A wavelength of emission that is not consistent with the wavelength anticipated from the properties of the compound. (3) An anomalous decay time and thermal quenching behaviour.

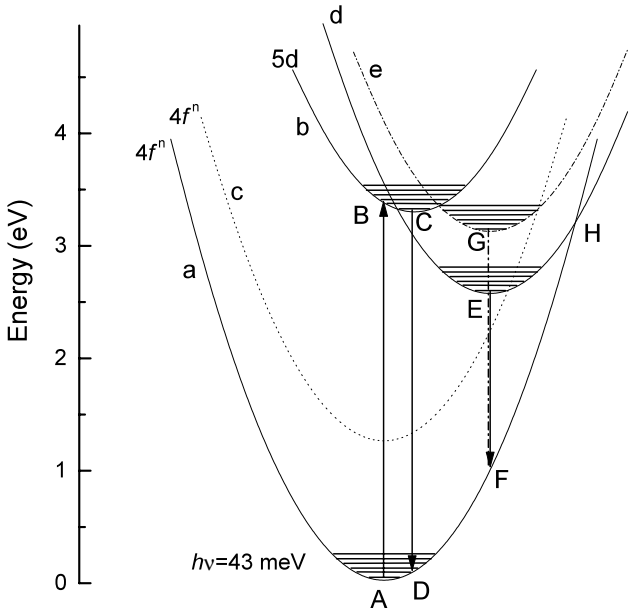

Figure 2. The configuration coordinate diagram illustrating normal df emission and anomalous emission. Energy values realistic for SrF_2 and BaF_2 were used with $h\nu = 43$ meV.

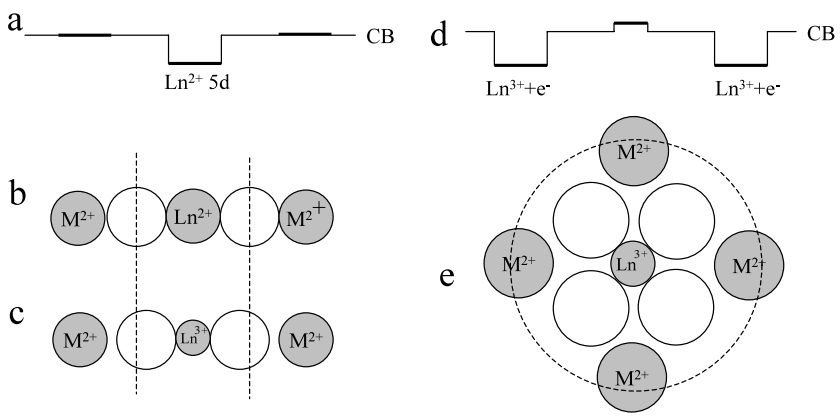

Figure 3. An illustration of the impurity-trapped exciton configuration in an MX_2 type of compound. (a) The occupied 5d energy level located just below the conduction band. (b) Ionic radii before the fd transition. (c) Ionic radii plus relaxation after autoionization. (d) Energy levels after autoionization and relaxation. (e) An electron orbiting around Ln^{3+} in the impurity-trapped exciton configuration.

Information on the width of the Eu^{2+} emission band, the Stokes shift, and how the two are related has been presented and discussed in [25]. Whenever these properties deviate strongly from normal values, it is an indication that conduction band levels may participate in the luminescence process. Employing such comparative methods, compounds showing anomalous emission were identified [25]. The information is reproduced in table 1. The wavelength of fd absorption, normal df emission, and anomalous emission are given together with the Stokes shift and the FWHM of the anomalous emission band. Compounds in which Eu^{2+} does not emit, even down to liquid helium temperature, are also compiled.

Table 1. Properties of Eu^{2+}-doped compounds with (suspected) anomalous luminescence. Wavelengths are in nanometres and Stokes shifts ΔS and widths Γ are in electron volts. Unless otherwise indicated, the width is specified at room temperature. 'xx' means that broadband emission is not observed down to ≈10 K.

Compound	λ_{abs}	λ_{em}^{df}	λ_{em}^{anom}	ΔS^{anom}	Γ_{Eu}^{anom}
BaF_2	382	403	590	1.14	0.51 (77 K)
$BaLiF_3$	333		410	0.70	0.37 (270 K)
CdF_2	407		xx		
$CsCaF_3$ (300 K)	425		510	0.49	0.60
$CsCaF_3$ (77 K)	425		610	0.88	0.48 (77 K)
$RbMgF_3$ (Rb)	340	365	405	0.59	0.40
$Ba_5(PO_4)_3F$ (6h)		432	475		
Sr_2LiSiO_4F	400		533	0.77	0.49
$Ba_2Y(BO_3)_2Cl$		538	634		0.30 (4 K)
Cs_2SO_4	378		450	0.52	0.66
HT-phase $Ba_3P_4O_{13}$			438		0.69
LT-phase $Ba_3P_4O_{13}$			570		0.71
δ-$Ba_2P_2O_7$			xx		
$Ba_2Mg(PO_4)_2$			585		0.54
$Ba_2Ca(PO_4)_2$		463	520		0.73
α-$Ca_3(PO_4)_2$			484		0.58
$Ba_2Ca(B_3O_6)_2$		450	495		
$Ba_2Mg(B_3O_6)_2$	390	425	476	0.57	0.43 (4 K)
$Ba_2LiB_5O_{10}$	375		630	1.34	0.30 (4 K)
I-SrB_2O_4	420		xx		
I-CaB_2O_4	350	368	477	0.94	0.35
$Sr_2B_2O_5$			xx		
$Ba_2Mg(BO_3)_2$	413		608	0.96	0.47
$Ba_2Ca(BO_3)_2$			521		
$BaLi(BO_3)$			510		
$Sr_2Mg(BO_3)_2$			590		
$Sr_3(BO_3)_2$	485		578	0.41	0.50 (4 K)
$Ca_3(BO_3)_2$			xx		
$BaAl_3BO_7$	350	360	458	0.84	0.63
$Sr_2Al_2B_2O_8$		415	529		
$Ba_2Si_3O_8$			485		
$BaSi_2O_5$			520		
$BaSiO_3$			550		
$BaMg(SiO_4)$	415	437	560	0.77	0.51 (4 K)
$Ba_2(SiO_4)$	434		505	0.40	0.29
$Sr_2(SiO_4)$	390	490	570	1.00	0.40
$BaGa_2O_4$			xx		
$SrGa_2O_4$			xx		
$BaHfO_3$ (4.2 K)	355		595	1.41	0.59
$BaHfO_3$ (220 K)	355		479	0.90	0.60
$SrZrO_3$			xx		
$Ba_4Ga_2S_7$	521		654	0.48	0.24 (80 K)
$Ba_2Ga_2S_5$			xx		
$Ba_5Ga_2S_8$			xx		

As a demonstration of how anomalous emission can be identified, figure 4 shows the wavelength of emission in Eu^{2+}-doped fluoride crystals. Data are displayed against the so-called compound identification number. Information on the meaning and relevance of this

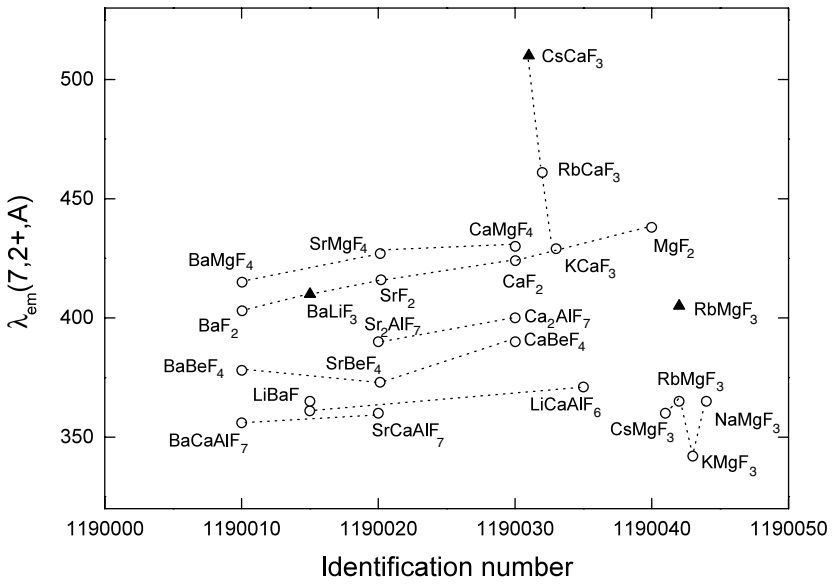

Figure 4. The wavelength of Eu^{2+} emission in fluoride compounds. For the meaning of the identification number, see [25, 27]. ○: normal df emission data; ▲: anomalous emission data.

number can be found in [25, 27]. Usually λ_{em} increases with decreasing size of the site occupied. This can be observed for the sequence BaF_2, SrF_2, CaF_2, and MgF_2, and several other sequences of data connected by dashed lines.

The large increase of λ_{em} in the sequence $KCaF_3$, $RbCaF_3$, and $CsCaF_3$ with Eu^{2+} on the Ca^{2+} site is unusual. The emission in $CsCaF_3$ also behaves strangely with increase of temperature, i.e., it shifts from 610 nm at 77 K to 510 nm at 300 K [28]. A similar blue-shift occurs in $BaHfO_3$ where there is a strongly Stokes-shifted wide emission band at 595 nm at 4.2 K and at 479 nm at room temperature [29]. Such behaviour can be well understood with the diagram in figure 2. Thermal activation from the impurity-trapped exciton state (point G) to the 5d state (point C) will accomplish such a blue-shift.

The 410 nm Eu^{2+} emission in $BaLiF_3$ was attributed to df emission [30]. The Stokes shift of 0.70 eV is, however, very large for Eu^{2+} and two times larger than that observed for $BaLiF_3$:Ce^{3+} [31]. Usually the Stokes shift for Eu^{2+} is significantly smaller than for Ce^{3+} [25, 27]. A close inspection of the emission spectrum of Eu^{2+} in $BaLiF_3$:Eu^{2+} at 270 K from [30] does reveal a weak band around 365 nm. This agrees with the anticipated location of normal df emission. For Eu^{2+} on the Rb site in $RbMgF_3$ an emission is observed at 405 nm which is at significantly longer wavelength than in equivalent compounds such as $CsMgF_3$ and $KMgF_3$. At 580 K an emission at 365 nm develops which can be tentatively attributed to the normal df emission [32].

2.2. Anomalous Yb^{2+} emission

A systematic search on the broadband luminescence of Yb^{2+} in compounds provided the data compiled in table 2. The wavelength λ_{abs}^{sf} of the spin-forbidden Yb^{2+} fd absorption band is in column 2. This band is always found ≈0.24 eV below the band of the first spin-allowed absorption [2]. Therefore, when only the spin-allowed transition is observed, one may estimate λ_{abs}^{sf}. Those estimated values are put within brackets in column 2. The wavelength of the spin-

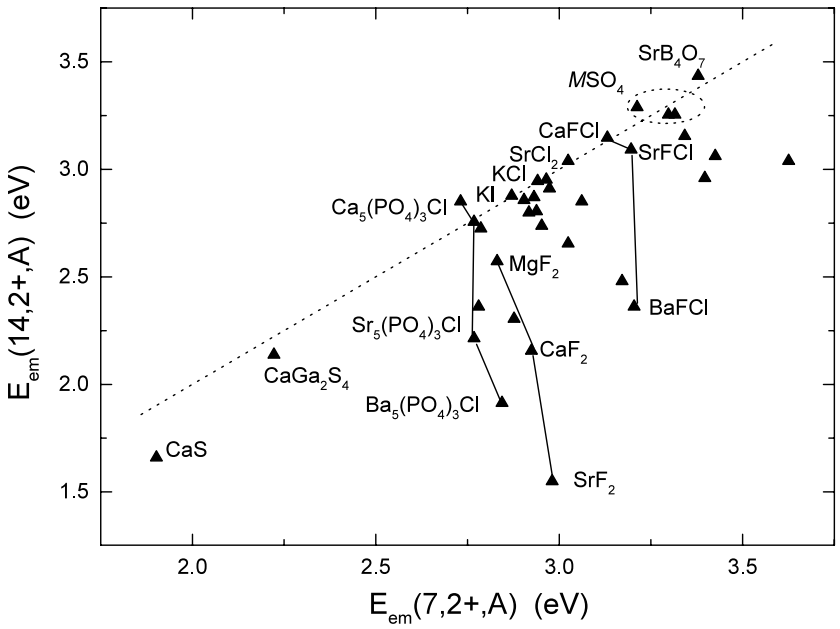

Figure 5. The energy of emission $E(14, 2+, A)$ of Yb^{2+} against that for Eu^{2+} ($n = 7$). The dashed line shows the expected relation between the two in the case of normal df emission.

forbidden emission is in column 3. Also, compounds in which Yb^{2+} does not emit, even down to liquid helium temperature, are listed. To identify those cases where conduction band states may play a role in the emission, information available on the df emission of Eu^{2+} in the same compounds will be used [25].

In [2] it was found that the spin-forbidden Yb^{2+} fd emission in a site in a compound is to be found within ± 0.1 eV of the energy of the spin-allowed fd emission of Eu^{2+} on the same site in the same compound. Data on df emission in Yb^{2+} are shown against emission in Eu^{2+} in figure 5. The dashed line indicates where the emission of Eu^{2+} is located. Data on $16Yb^{2+}$-doped compounds do indeed fall within the standard deviation of ± 0.1 eV from this line. The majority of data, however, fall well below, and no data fall significantly above. The magnitudes of the deviation ΔD are compiled in table 2. Whenever ΔD is less than -0.1 eV, conduction band states are likely to be involved in the emission. Note that the FWHM of the anomalous emission varies between 0.35 and 0.75 eV, which is two times larger than usually observed for normal df emission [25].

Inspecting the data, several trends are observed.

(1) ΔD (see column 5 in table 2) tends to become more negative with increasing size of the cation site occupied by Yb^{2+}. This can be observed for the sequences (MgF_2, CaF_2, SrF_2), (CaFCl, SrFCl, BaFCl), and ($Ca_5(PO_4)_3Cl$, $Sr_5(PO_4)_3Cl$, $Ba_5(PO_4)_3Cl$). These compounds are connected by line segments in figure 5.

(2) In the sequence: sulfates, phosphates, borates, silicates, aluminates, 'simple' oxides, the binding of oxygen ligands tends to decrease. In the same sequence the probability of observing normal df emission decreases and the probability of observing anomalous emission or no emission at all increases. Normal df emission is only observed in the sulfates MSO_4 (M = Ca, Sr, Ba) and in the condensed borate SrB_4O_7. Anomalous emission occurs in several phosphates and few silicates, but not in aluminates and CaO. In aluminates and 'simple oxides', even down to 4 K, no broadband Yb^{2+} emission has been reported.

Table 2. Broadband emission in Yb^{2+}-doped compounds. The wavelengths of the spin-forbidden df absorption λ_{abs}^{sf} and broadband emission λ_{em} are in nm. Values for λ_{abs}^{sf} within brackets are estimates based on spin-allowed absorption wavelengths. The FWHMs Γ_{Yb} and deviations ΔD are in electron volts. Unless otherwise specified, the width is at room temperature. xx means that broadband emission is not observed down to ≈10 K.

Compound	λ_{abs}^{sf}	λ_{em}	Γ_{Yb}	ΔD	References
BaF_2	(380)	xx			[4, 12]
$BaLiF_3$	330	467	0.367	−0.37	[45]
$SrAlF_5$	(330)	405	0.446	−0.36	[46]
SrF_2	375	800	0.595 (4.2 K)	−1.43	[11, 12]
$LiSrAlF_6$		440	0.657		[47]
CaF_2	390	575	0.508 (150 K)	−0.77	[12, 48, 49]
$LiCaAlF_6$	(350)	393	0.409	−0.19	[47]
MgF_2	420	482	0.508	−0.26	[15, 47]
$KMgF_3$	309	408	0.496	−0.59	[15, 47]
$NaMgF_3$	327	419	0.682	−0.44	[15]
BaFCl		525		−0.84	[50]
SrFCl	(335)	401	0.171 (4.2 K)	−0.10	[50]
CaFCl	344	394	0.241 (4.2 K)	0.02	[50]
RbCl	(401)	426	0.099 (15 K)	−0.06	[51]
KCl	416	432	0.172	−0.06	[52–54]
NaCl	423	434	0.124	−0.05	[11, 55]
Cubic $SrCl_2$	394	408	0.097 (4.2 K)	0.01	[11, 56]
BaFBr		500	0.372 (4.2 K)	−0.69	[50]
SrFBr	(363)	416	0.186 (4.2 K)		[50]
CaFBr	(392)	410	0.114 (4.2 K)		[50]
KBr	418	442		−0.12	[51, 52, 54, 57]
KI	(417)	431	0.053 (10 K)	0.01	[57]
$Ba_5(PO_4)_3Cl$	(412)	648	0.471	−0.93	[58]
$Sr_5(PO_4)_3Cl$	(427)	450	0.154 (77 K)	−0.01	[58]
$Sr_5(PO_4)_3Cl$	(427)	560	0.608	−0.55	[58]
$Ca_5(PO_4)_3Cl$		435	0.112 (77 K)	0.12	[58]
Ca_2PO_4Cl		455	0.186 (77 K)	−0.06	[58]
$Sr_2B_5O_9Cl$	(410)	420	0.281	−0.01	[59]
$Sr_2B_5O_9Br$	(404)	421	0.360	0.00	[59]
$BaSO_4$	346	381	0.226 (160 K)	−0.06	[14]
$SrSO_4$	346	381	0.193 (160 K)	−0.04	[14]
$CaSO_4$	365	377	0.126 (110 K)	0.08	[14]
α-$Ba_2P_2O_7$		xx			[17]
α-$Sr_2P_2O_7$	380	453	0.273 (4.2 K)	−0.22	[17]
$Ba_3(PO_4)_2$	(384)	435	0.181 (4.2 K)	−0.21	[17]
$Sr_3(PO_4)_2$	400	442	0.211 (4.2 K)	−0.13	[17, 58]
SrB_4O_7	350	361	0.166	0.06	[60, 61]
$Ba_2(SiO_4)$		xx			[17]
$Sr_2(SiO_4)$		xx			[17]
$CaB(OH)(SiO_4)$	(393)	525	≈0.620	−0.42	[62, 63]
$CaB_2O(Si_2O_7)$	(390)	538	0.459	−0.57	[62]
β-$Ca_2(SiO_4)$		xx			[17]
$BaAl_2O_4$		xx			[17]
$SrAl_2O_4$		xx			[17]
$SrAl_{12}O_{19}$		xx			[17]
$CaAl_2O_4$		xx			[17]
$CaAl_4O_7$		xx			[17]
$CaAl_{12}O_{19}$		xx			[17]

Table 2. (Continued.)

Compound	λ_{abs}^{sf}	λ_{em}	Γ_{Yb}	ΔD	References
CaO		xx			[17]
$CaGa_2S_4$		580	0.239	−0.08	[64]
CaS	(659)	747	0.310	−0.24	[65]

(3) Most compounds for which normal df emission is observed contain large halogen ions, i.e., KI, KCl, NaCl, $SrCl_2$, CaFCl, $Ca_5(PO_4)_3Cl$, $Sr_2B_5O_9Br$, Ca_2PO_4Cl, $Sr_5(PO_4)_3Cl$, $Sr_2B_5O_9Cl$, and $CaGa_2S_4$. None of the fluoride compounds show normal Yb^{2+} df emission.

These three trends for Yb^{2+} are consistent with that for the Eu^{2+}-doped compounds. In most compounds with anomalous Eu^{2+} emission, the Eu^{2+} ion is on the large Ba site, which is consistent with trend (1). Trend (2) with the binding strength of the oxygen ligands can also be observed for Eu^{2+} on Ba sites in oxides. The sulfates $BaSO_4$ and $BaMgSO_4$ show df emission [25], but in proceeding to phosphates, borates, silicates, and aluminates, the number of compounds showing anomalous emission or no emission at all increases. Trend (3) is supported by the fact that table 1 does not contain any chloride, bromide, or iodide compounds, and apart from a few thio-gallates, all known Eu^{2+}-doped sulfides, selenides, and nitrides show normal df emission.

Comparing the data on Eu^{2+} with those on Yb^{2+}, another trend (trend (4)) appears, i.e., 'anomalous' emission is much more frequently observed when the small Yb^{2+} is the dopant than when Eu^{2+} is the dopant. In fact, it appears that whenever emission in Eu^{2+} is anomalous, emission of Yb^{2+} is likely to be fully absent. A final trend (trend (5)) can be formulated as: 'normal df emission is never observed for divalent lanthanides on trivalent cation sites and always observed for divalent lanthanides on monovalent cation sites'.

3. Discussion

To understand when anomalous emission can be expected, information is needed on the energy difference I_d between the lowest 5d level and the bottom of the conduction band. By analogy to [39], this can be expressed as

$$I_d(n, Q, A) = I_d(n, Q, \text{free}) - E_{MP}(A) - E_{pol}^{5d}(A) - E_{CB}(A) \quad (2)$$

where $I_d(n, Q, \text{free})$ is the 5d ionization energy in the free lanthanide, E_{MP} is a contribution due to the Madelung energy at the lanthanide site. A possible contribution from the Pauling repulsion between 5d electron and anion ligands is also included in this term. E_{pol}^{5d} is caused by the polarization due to the removal of a 5d electron from the lanthanide site. A strongly polarizable host lattice reduces the ionization potential because of effective shielding of the hole left by the removed electron. $E_{CB}(A)$ is the electron affinity in the conduction band of the crystal.

We first assume that the binding energy in the free ion and the interaction between 5d electron and crystalline surroundings do not depend on n. We will also ignore the lanthanide contraction with increasing n and related lattice relaxation. Under these conditions, $I_d(n, Q, A)$ is constant with varying n. Using the divalent lanthanides in SrF_2 as an example, we arrive at the situation shown in figure 6 where a value of 0.614 eV is used for I_d. The top of the valence band is chosen as the zero of energy. The bottom of the conduction band E_{CB} is located around 11.4 eV [33]. The dashed horizontal lines in figure 6 represent the onset of

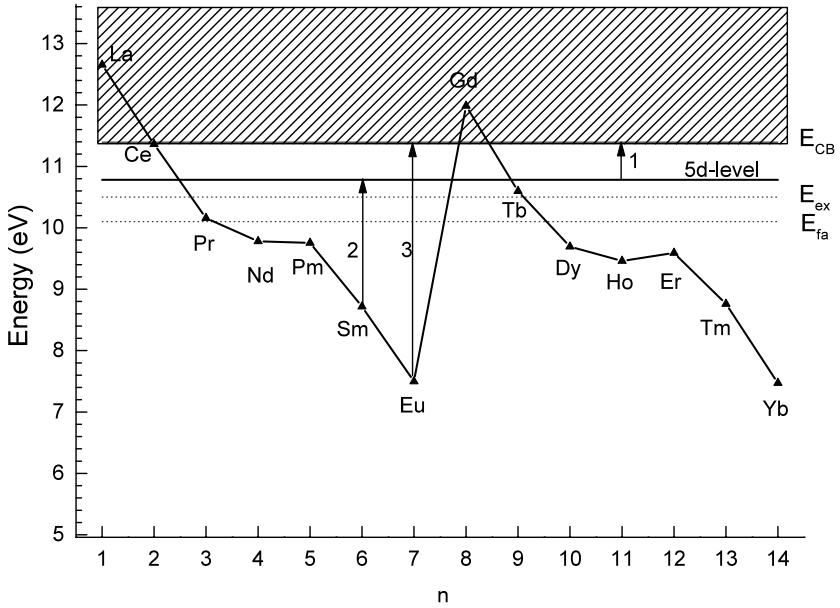

Figure 6. An idealized scheme showing the energy levels of the divalent lanthanides in SrF_2. Arrow 1: $I_d(11, 2+, SrF_2)$; arrow 2: $E_{abs}(6, 2+, SrF_2)$; arrow 3: $I_f(7, 2+, SrF_2)$.

the fundamental absorption E_{fa} in SrF_2 at 10.1 eV and the location of the exciton peak E_{ex} at 10.5 eV in the spectra.

Using equation (1), one may write for the ionization energy of the $4f^n$ ground state

$$I_f(n, Q, A) = I_d(n, Q, A) + E_{A\,free}(n, Q) - D(Q, A). \tag{3}$$

With $D(2+, SrF_2) = 1.03$ eV from [2] and $E_{A\,free}$ from table 3, the 4f ground state levels can be drawn as in figure 6. The observation that anomalous luminescence in Yb^{2+} is much more probable than in Eu^{2+} (trend (4)) indicates that $I_d(14, 2+, A)$ should be smaller than $I_d(7, 2+, A)$. Clearly, the initial assumption that I_d is constant with varying n has to be abandoned.

From data on level energies and ionization energies for the free divalent lanthanides as compiled by Sugar and Reader [34], the ionization energy of the $4f^n5d^0$ configuration and the $4f^{n-1}5d^1$ configuration were determined. The results are shown in figure 7. Starting from La^{2+} up to Gd^{2+}, the 5d ionization energy increases by about 1.5 eV. Further on, from Gd^{2+} to Yb^{2+}, it remains relatively constant.

Two contributions to the 5d electron ionization energy in the free lanthanides will be considered. These are the Coulomb attraction $E_C(n, Q, A)$ between the 5d and the $[Xe]4f^{n-1}$ core, and the isotropic exchange interaction $E_{ex}(n, Q, A)$ between the 5d electron spin and total spin of the $n - 1$ electrons remaining in the 4f shell. As also suggested by Sekiya *et al* [35], the Coulomb attraction is expected to increase with decreasing size of the lanthanide ion. We can make a crude approximation by considering the Coulomb attraction between a 5d electron at a distance R (pm) from a hole in the centre of the lanthanide:

$$E_C(n, Q, A) = -\frac{Z_h q}{4\pi\epsilon_0}\frac{1}{R} \approx \frac{-1440 Z_h}{R}\ \text{eV} \tag{4}$$

where Z_h is the effective charge of the hole in units of the elementary charge q.

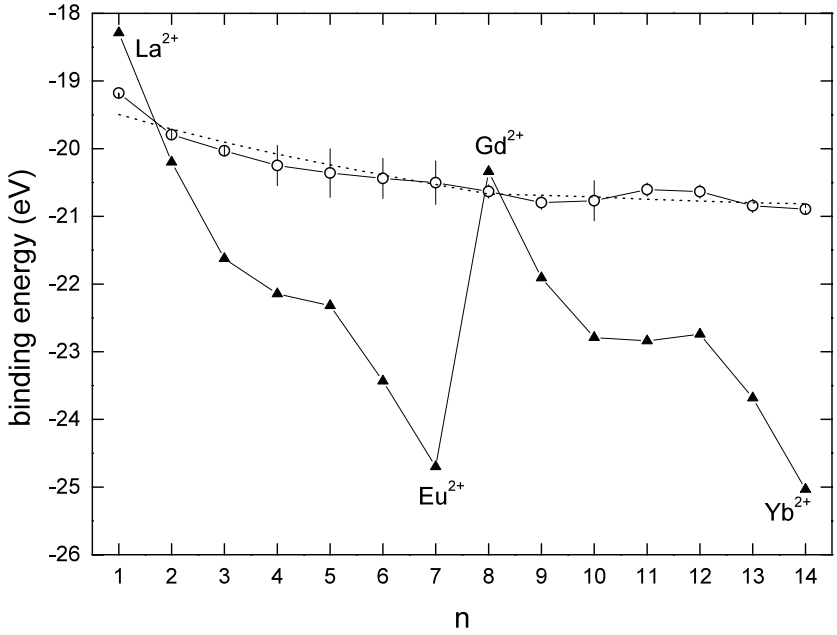

Figure 7. ▲: the energy of the $4f^n$ ground state in the free divalent lanthanides. ○: the energy of the lowest $4f^{n-1}5d$ level in the free divalent lanthanides. Data were obtained from the ionization energies compiled in [34]. The dashed curve is from calculations in this work.

Table 3. $E_{A\,\mathrm{free}}$-values from [2]. The Coulomb and exchange correction values pertain to the free divalent lanthanides. The Madelung correction values were calculated for SrF_2. The last column shows the sum of all three correction terms. All energies are in electron volts.

Ln	n	$E_{A\,\mathrm{free}}(n, 2+)$	$\Delta E_{\mathrm{C}}(n, 2+, \mathrm{free})$	$\Delta E_{\mathrm{ex}}(n, 2+, \mathrm{free})$	$\Delta E_{\mathrm{M}}(n, 2+, SrF_2)$	$\Delta E_{\mathrm{cor}}^{\mathrm{calc}}$
La	1	−0.942	−0.644	−0.391	0.991	−0.044
Ce	2	0.351	−0.531	−0.285	0.811	−0.005
Pr	3	1.556	−0.420	−0.205	0.637	0.012
Nd	4	1.934	−0.311	−0.136	0.468	0.021
Pm	5	1.959	−0.204	−0.085	0.305	0.016
Sm	6	2.996	−0.100	−0.038	0.149	0.011
Eu	7	4.216	0	0	0	0
Gd	8	−0.273	0.098	0.045	−0.143	−0.001
Tb	9	1.116	0.192	−0.031	−0.280	−0.118
Dy	10	2.021	0.283	−0.098	−0.410	−0.225
Ho	11	2.254	0.370	−0.151	−0.533	−0.315
Er	12	2.124	0.453	−0.206	−0.649	−0.402
Tm	13	2.952	0.531	−0.259	−0.757	−0.486
Yb	14	4.241	0.605	−0.319	−0.859	−0.574

Figure 8 shows the ionic radii of divalent, trivalent, and tetravalent lanthanides in compounds. The so-called crystal radius (CR) on sites with eightfold coordination from the compilation of data by Shannon was used [36]. A polynomial function of degree 2 is fitted through the data for the trivalent lanthanides. The same polynomial shifted by +18.7 pm can be used to estimate the radii for the divalent lanthanides. A downward shift by 18.1 pm provides the values for the tetravalent lanthanides.

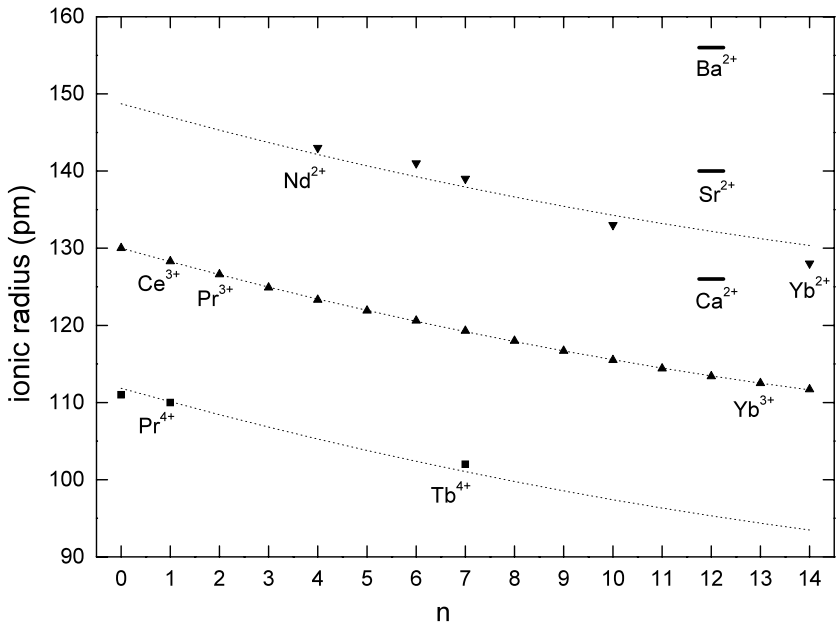

Figure 8. The ionic radii of the divalent, trivalent, and tetravalent lanthanides at sites with eightfold coordination (from [36]). The horizontal bars indicate the ionic radii of Ca^{2+}, Sr^{2+}, and Ba^{2+}.

Figure 9 and table 3 show the calculated differences $\Delta E_C(n, 2+, A) \equiv E_C(7, 2+, A) - E_C(n, 2+, A)$ for the free ions. They show that the Coulomb attraction in La^{2+} is 0.644 eV weaker than in Eu^{2+}, which in turn is 0.605 eV weaker than that in Yb^{2+}. On the basis of this correction term alone, the 5d ionization energy is predicted to be largest for Yb^{2+}.

The isotropic exchange interaction is given by [37, 38]

$$E_{ex} = -2J_0\vec{s}_d \cdot \vec{S}_f \tag{5}$$

where J_0 expresses the strength of the exchange interaction, $\vec{s}_d = 1/2$ is the spin of the 5d electron, and $\vec{S}_f$ is the total spin of the electrons in the ground state of the $4f^{n-1}$ core. Figure 9 and table 3 show the calculated differences $\Delta E_{ex}(n, 2+, A) \equiv E_{ex}(7, 2+, A) - E_{ex}(n, 2+, A)$. The values for J_0 estimated by Yanase for the free divalent lanthanide ions were used [37]. The exchange interaction is largest for Gd^{2+} with seven aligned spins in the $4f^{n-1}$ core. Going to both ends of the lanthanide series, the exchange interaction decreases, leading to smaller 5d electron binding.

In figure 7 the combined effect of Coulomb and exchange interaction in the free ions is shown by the dashed curve. In fact, the Coulomb plus exchange interaction yields an ionization energy that is still 10 eV smaller than that observed experimentally. However, since the absolute value is not of real interest in this work, the total energy was shifted by this amount to make it coincide with experimental values. The variation with n, which is of most interest, is rather well reproduced. We now interpret the increase of 5d binding from $n = 1$ to 8 as an increasing Coulomb attraction augmented with the exchange interaction. For $n > 8$ the Coulomb attraction still increases but the exchange interaction decreases and I_d is relatively constant.

The conclusion from the anomalous emission study that $I_d(14, 2+, A) < I_d(7, 2+, A)$ is not supported by the free ion data. In compounds, due to the charge cloud expansion (nephelauxetic effect) of the 5d orbital, it is expected that the Coulomb attraction will decrease.

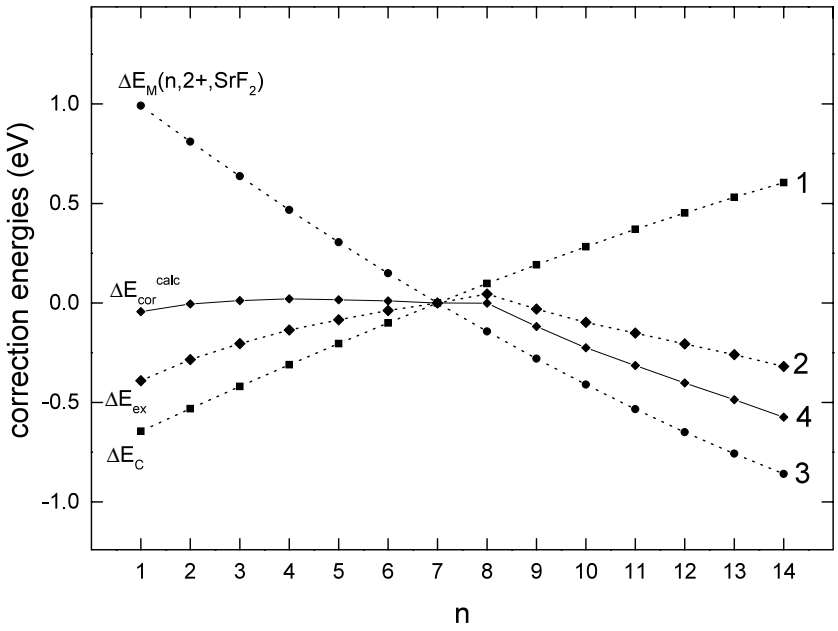

Figure 9. The calculated correction to the constant 5d ionization energies. Dashed curve 1: $\Delta E_{\rm C}(n, 2+, \text{free})$. Dashed curve 2: $\Delta E_{\rm ex}(n, 2+, \text{free})$. Dashed curve 3: $\Delta E_{\rm M}(n, 2+, \text{SrF}_2)$. Solid curve 4 is the sum of curves 1, 2, and 3.

Larger polarizability of the host lattice may also cause a decrease of the Coulomb interaction because of screening effects and a smaller effective $Z_{\rm h}$ in equation (4). Despite this and possible changes in the size of the exchange interaction with type of compound, we still do not arrive at $I_{\rm d}(14, 2+, A) < I_{\rm d}(7, 2+, A)$ which would explain trend (4).

To further resolve this issue, experimental data are needed on either $I_{\rm d}(n, Q, A)$ or $I_{\rm f}(n, Q, A)$ and on the band gap. Values for $I_{\rm f}(n, Q, A)$ have been determined for several divalent lanthanides in CaF_2, SrF_2, and BaF_2 by means of photoconductivity experiments [9, 10, 13, 39, 40]. To explain the data, the following electrostatic model was proposed [39]:

$$I_{\rm f}(n, Q, A) = I_{\rm f}(n, Q, \text{free}) - E_{\rm MP}(A) - E^{\rm 4f}_{\rm pol}(A) - E_{\rm CB}(A) - E^{\rm cor}_{\rm M}(n, Q, A) - E^{\rm cor}_{\rm P}(n, Q, A) \quad (6)$$

where the meaning of the first four terms is similar to that in equation (2). $E^{\rm cor}_{\rm M}$ and $E^{\rm cor}_{\rm P}$ are corrections to the Madelung energy and Pauling repulsion due to lattice relaxation around the lanthanide ion, respectively. Assuming an electrostatic point charge model, $E^{\rm cor}_{\rm M}$ can be expressed as [9, 39]

$$E^{\rm cor}_{\rm M} = \frac{NZ_{\rm eff}q}{4\pi\epsilon_0}\frac{f\,\Delta R}{R(R - f\,\Delta R)} \quad (7)$$

where N is the number of anion neighbours each with effective charge $Z_{\rm eff}$, R their distance to the central lanthanide in the unrelaxed lattice. $f\,\Delta R$ is the inward or outward relaxation of the surrounding anions. ΔR is defined (unlike in [39]) as the difference between the ionic radius of the substituted cation and the ionic radius of the lanthanide. It is positive for too large a cation site. In this work the correction term will be applied to the fluorites CaF_2, SrF_2, and BaF_2 where $f \approx 0.6 \pm 0.1$; see [39] and references therein. Note: a similar relaxation model with $f = 0.6$ was used for trivalent lanthanides in compounds [41].

A simple expression for E_P^{cor} is not available. However, when anions relax towards the lanthanide ion the exchange interaction between the 5d and the anion ligands increases leading to larger Pauling repulsion. Therefore the sign of E_P^{cor} is the same as that of E_M^{cor}.

To describe the variation of I_d with n, we write

$$I_d(n, 2+, A) = I_d(7, 2+, A) + \Delta E_M(n, 2+, A) + \Delta E_P(n, 2+, A) + \Delta E_C(n, 2+, A) + \Delta E_{ex}(n, 2+, A) \quad (8)$$

where the ionization energy of the 5d electron in Eu^{2+} is used as a common reference. ΔE_{ex} and ΔE_C were defined above, $\Delta E_M(n, 2+, A) \equiv E_M^{cor}(7, 2+, A) - E_M^{cor}(n, 2+, A)$. To a good approximation,

$$\Delta E_M(n, Q, A) \approx \frac{NZ_{eff}q}{4\pi\epsilon_0} \frac{f(R_{Ln} - R_{Eu})}{R(R - f\,\Delta R_{Eu})} \quad (9)$$

where $R_{Ln} - R_{Eu}$ are the differences in ionic radius that can be obtained from figure 8. ΔR_{Eu} is the size difference between Eu^{2+} and the replaced cation.

$\Delta E_M(n, 2+, SrF_2)$, obtained using $R = 250$ pm, $Z_{eff} = 1$, and $N = 8$, is shown in figure 9 and compiled in table 3. The lattice relaxation lowers the 5d levels of La^{2+} by 0.991 eV and lifts that of Yb^{2+} by 0.859 eV relative to those of Eu^{2+}. Qualitatively, it is expected that the Pauling repulsion will decrease with decreasing size of the lanthanide ion, which implies that the binding in Yb^{2+} is enhanced relative to that in Eu^{2+}. Although the magnitude of ΔE_P is not known, it will, like ΔE_C, oppose the effect of the Madelung correction ΔE_M.

If we neglect the effect of ΔE_P and use the free ion values for ΔE_C and ΔE_{ex}, the level scheme for the divalent lanthanides in SrF_2 as shown in figure 10 is obtained. The total correction values used are listed as ΔE_{cor}^{calc} in table 3 and are shown as solid curve 4 in figure 9. We have now arrived at a situation where $I_d(14, 2+, A) > I_d(7, 2+, A)$ which is required to explain trend (4)—that anomalous emission is more probable for Yb^{2+} than for Eu^{2+}.

Both the Madelung correction and the Coulomb correction are based on crude models, and a model for the Pauling correction was not employed. Furthermore, since Coulomb and exchange interactions are anticipated to decrease in compounds, a large error in the magnitudes of the corrections can be present. At this stage we conclude that the Coulomb and Pauling corrections tend to cancel against the Madelung correction. It seems that the overall correction follows more or less the curve shown for I_d in figure 10 with a minimum near Eu^{2+} and Gd^{2+}.

Employing the same method as for SrF_2, the divalent lanthanide level schemes in BaF_2 and CaF_2 can be constructed; see figures 11 and 12. The Madelung corrections were calculated with $R = 269$ and 237 pm. We further used $D(2+, CaF_2) = 1.128$ eV and $D(2+, BaF_2) = 0.988$ eV. $I_d(7, 2+, BaF_2) = -0.196$ eV and $I_d(7, 2+, CaF_2) = 0.846$ eV where chosen so as to comply with the results on the anomalous emission and results from other experiments; see section 4. In the three fluorites the variations of I_d with n are very similar. For $n < 8$, $\Delta E_M(n, 2+, MF_2)$ almost fully cancels the exchange and Coulomb corrections, and the 5d ionization energy is practically constant. From $n = 8$ to 14 the ionization energy decreases, and the 5d ionization energy of Yb^{2+} is about 0.56 eV smaller than that of Eu^{2+}.

Trend (1)—that *anomalous emission is more probable for the lanthanides on the large Ba site than on the small Ca site*—is seen in figures 10–12 as an increase in the 5d electron binding energy $I_d(7, 2+, MF_2)$. $I_d(7, 2+, BaF_2)$ was chosen such that the 5d level of Eu^{2+} is just inside the conduction band leading to anomalous emission. Normal df emission has also been observed [26]—see table 1—which means that the *relaxed* 5d state may be located just below the bottom of the conduction band. The emission is fully quenched for Yb^{2+} because it is located far above the bottom of the conduction band. In SrF_2 and CaF_2 the 5d level of Eu^{2+} is well below and normal emission is observed. However, 5d for Yb^{2+} is much closer to the

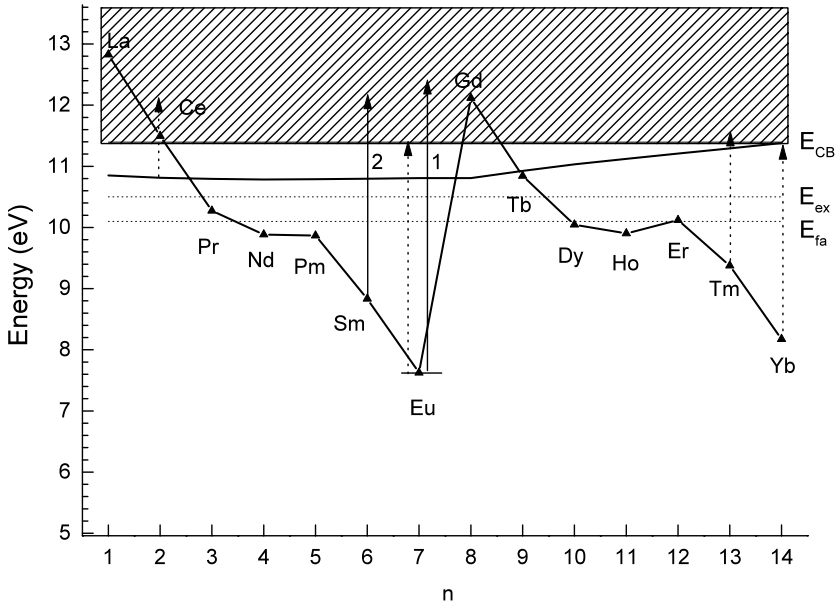

Figure 10. A scheme showing the $4f^n$ ground state and lowest 5d energy levels of the divalent lanthanides in SrF_2, $I_f(7, 2+, SrF_2)$. The arrows indicate reported photoconductivity ionization thresholds. The fundamental absorption edge and the exciton energy are indicated by dashed horizontal lines.

conduction band, leading again to anomalous emission. The deviation ΔD in table 2 is largest for SrF_2.

The increase of I_d with decreasing cation site size can be related to the correction term E_M^c in equation (6). Ba^{2+} is 30 pm larger than Ca^{2+}. If everything else were to remain the same, equation (7) would predict for a lanthanide on a Ba^{2+} site an about 1–1.5 eV smaller value for I_d than for on a Ca site. This agrees more or less with the level schemes in figures 10–12. However, in reality E_{MP}, E_{pol}^{5d} and E_{CB} in equation (2) do change and the situation is more complicated. Only when these parameters influence the electronic levels of the lanthanide in the same way as they influence the conduction band levels does E_M^{cor} remain the most important parameter for explaining trend (1).

Trend (2)—that *the probability of anomalous emission or the absence of emission increases with decreasing binding of the oxygen ligands*—can have different causes. Decreasing binding of oxygen ligands is related with increasing covalency between lanthanide and anions. Each of the parameters E_{MP}, E_{pol}^{5d}, E_{CB}, and indirectly also the red-shift $D(2+, A)$, may be involved in this. Clearly a diversity of effects have to be taking into account. The same applies to trend (3)—that *the probability of anomalous emission tends to increase with decreasing size of the anion*. For Yb^{2+}, it may be related to the Madelung correction term because the R^{-2}-dependence leads to small corrections for the large anions Cl, Br, I, and S. Furthermore, the Madelung potential diminishes with increasing covalency between anions and cations. In equation (9) this translates into a decreasing value for Z_{eff}. There may be other contributions, and only by acquiring knowledge of I_d for many different compounds and lanthanides may one hope to disentangle all the different contributions.

When a divalent lanthanide is located on a monovalent cation site, effectively the 5d electron is bonded to a lanthanide with excess positive charge. Coulomb attraction will be

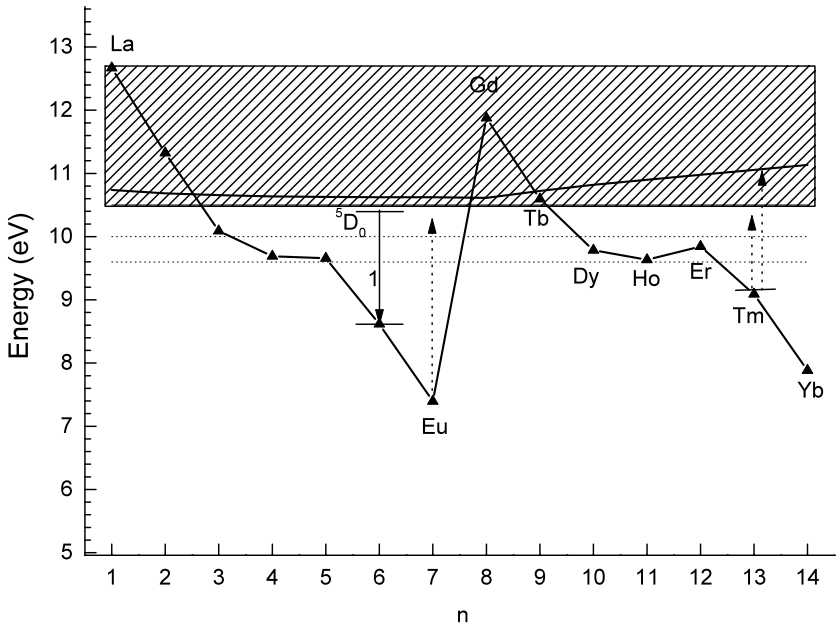

Figure 11. A scheme showing the $4f^n$ ground state and the lowest 5d energy levels of the divalent lanthanides in BaF_2. Arrow 1 represents the $^5D_0 \rightarrow {}^7F_0$ transition in Sm^{2+}. Dashed arrows indicate photoconductivity ionization thresholds. The fundamental absorption edge and the exciton energy are indicated by dashed horizontal lines.

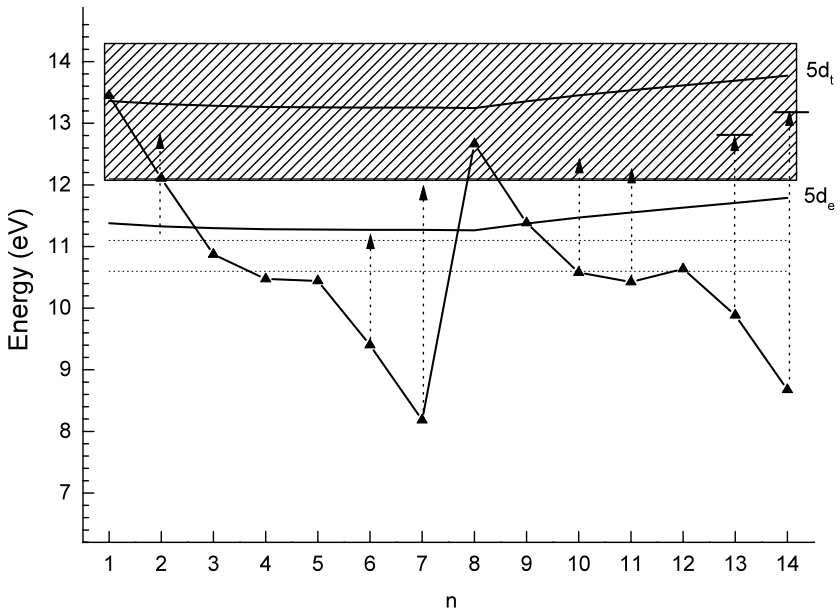

Figure 12. A scheme showing the $4f^n$ ground state levels and the doublet $5d_e$ and triplet $5d_t$ levels of the divalent lanthanides in CaF_2. Dashed arrows indicate photoconductivity ionization thresholds. The fundamental absorption edge and the exciton energy are indicated by dashed horizontal lines.

strong, leading to large I_d. Experimentally, this is evidenced by the occurrence of normal spin-allowed and spin-forbidden df emission of Yb^{2+} in KI, KBr, and KCl. Anomalous emission has not been observed on monovalent cation sites (trend (5)). When the divalent lanthanide is on a trivalent cation site, there is a lack of positive charge. Coulomb attraction is small and the 5d level is located above the top of the conduction band. Experimentally, this is evidenced by the fact that df emission of Eu^{2+} is never observed on trivalent sites (trend (5)) [25].

Sm^{2+} and Tm^{2+} are the only lanthanides besides Eu^{2+} and Yb^{2+} for which normal df emission has been observed [2]. Tm^{2+} is next to Yb^{2+} in the lanthanide series and $I_d(13, 2+, A)$ is expected to be slightly larger than $I_d(14, 2+, A)$. This means that when normal df emission is observed for Yb^{2+}, it will most likely also be observed for Tm^{2+}. In most compounds, however, as for Yb^{2+}, autoionization of the Tm^{2+} 5d is a likely process. The only compounds for which Tm^{2+} df emission has been reported are $SrZnCl_4$, $BaZnCl_4$, $SrCl_2$, SrB_4O_7. The last two compounds also show normal Yb^{2+} emission. The others contain large chlorine anions in accordance with trend (3).

Sm^{2+} has about the same ionic radius as Eu^{2+}, and $I_d(6, 2+, A)$ is expected to be quite similar to $I_d(7, 2+, A)$. Therefore, when Eu^{2+} shows normal df emission, Sm^{2+} will also show normal df emission. Indeed, in displaying data on Sm^{2+} as in figure 5, all data fall nicely on the anticipated line; see [25].

4. Related phenomena

Anomalous luminescence is very common for Yb^{2+} on a divalent site such as the Ca^{2+} and Sr^{2+} sites, whereas for the Yb^{2+} and a large Ba^{2+} site there is often no emission at all. Apparently $I_d(14, 2+, A)$ is always close to zero or negative. This implies that the lowest 5d state of the other divalent lanthanides is within $\approx$1.2 eV from the bottom of the conduction band. Furthermore, since the total crystal field splitting of the 5d configuration is usually larger than 1.2 eV, the higher-energy $4f^{n-1}5d$ levels are to be found inside the conduction band. For CaF_2 with $10Dq = 2.05$ eV this is illustrated in figure 12 [26].

States located inside or very close to the conduction band have a very short lifetime because of the rapid relaxation or thermal excitation to conduction band levels. The short lifetime leads to the absence of vibrational structure in fd excitation or absorption bands. The presence or absence of such vibrational structure therefore provides clues to the location of 5d bands. It is for example known that vibrational structure is absent in the lowest fd absorption bands of Sm^{2+} and Eu^{2+} in BaF_2 [42, 43]. It is also absent for Eu^{2+} in SrF_2, but the vibrational structure is clearly observed in the lowest 5d band in CaF_2:Eu^{2+} [26]. Although one may not exclude the possibility of a fast relaxation from the 5d state to the impurity-trapped exciton state, the absence or presence of vibrational structure clearly provides information on the location of 5d levels.

One may use other information to locate energy levels. In BaF_2 the $4f^6[^5D_0]$ level of Sm^{2+} is located below the lowest 5d level; see figure 11. The ff emission from this level is thermally quenched with an activation energy of 0.134 eV attributed to ionization of the $^5D_0$ level [42]. Apparently, the $^5D_0$ level is located just below the bottom of the conduction band. This is the situation shown in figure 11.

Thermal quenching of normal df luminescence via autoionization can also be used to localize impurity energy levels relative to the conduction band bottom. Lizzo *et al* [14] used this method to position the lowest 5d bands of Yb^{2+} in $CaSO_4$ and SrB_4O_7 some 0.40 and 0.43 eV below the conduction band, respectively. It was also observed that Yb^{2+} emission quenches at lower temperature than Eu^{2+} emission [17], which is evidently related to $I_d(14, 2+, A) < I_d(7, 2+, A)$. The temperature $T_{0.5}$ where the df emission of Eu^{2+} is quenched to half its value is at 295 and 360 K for SrF_2 and CaF_2, respectively [5]. The higher quenching

temperature for CaF_2 indicates that $I_d(7, 2+, CaF_2) > I_d(7, 2+, SrF_2)$ in line with figures 10 and 12.

One of the few direct methods for locating energy levels is by means of photoconductivity experiments. The dashed arrows in figures 10–12 indicate the threshold energy needed to photoionize the ground state of the divalent lanthanides [9, 10, 12, 13, 39]. Those for Eu^{2+}, Tm^{2+}, and Yb^{2+} in SrF_2 coincide well with the bottom of the conduction band. The same applies for Eu^{2+} and Tm^{2+} in BaF_2 and for Eu^{2+}, Dy^{2+}, and Ho^{2+} in CaF_2.

The photoconductivity threshold in CaF_2:Yb^{2+} coincides with the dipole-allowed transition to the $4f^{13}[^2F_{5/2}]5d_e$ level at $\approx$1.24 eV higher energy than the $4f^{13}[^2F_{7/2}]5d_e$ level [12]. The oscillator strength for a direct transition from the localized $4f^n$ level to the delocalized conduction band levels is probably too small to generate a significant photocurrent. The onset for photoconductivity in CaF_2:Tm^{2+} coincides with an absorption at 450 nm [9, 44]. The threshold can be attributed to the dipole-allowed transition to the $4f^{12}[^3F_4]5d_e$ level located 0.87 eV above the lowest 5d level. Again direct transition to the bottom of the conduction band does not lead to a significant photocurrent. This illustrates that the photoconductivity threshold does not need to coincide with the direct transition to the bottom of the conduction band.

Photoionization thresholds for Ce^{2+} in BaF_2, SrF_2, and SrF_2 also do not agree with the expected ionization energies. Possibly figures 10–12 suggest too small an ionization energy for the large lanthanides, but this may also be related to the fact that the ground state configuration of Ce^{2+} in these compounds is the 4f5d configuration and not the $4f^2$ configuration. Lattice relaxation around Ce^{2+} and the related Madelung potential is then different, leading to electronic level shifts. In the scheme of figure 11, the ground state of Ce^{2+} is above the bottom of the conduction band in BaF_2. Contrary to the situation in SrF_2 and CaF_2, Ce^{2+} would not be stable against autoionization. Nevertheless, a photoconductivity threshold of 1.1 eV has been reported for Ce^{2+} in BaF_2 [39]. Apparently, Ce^{2+} is somehow stabilized, possibly by defects, leading to lower positioning of energy levels.

The photoconductivity threshold of Sm^{2+} in CaF_2 is clearly too small. This was also noticed by Pedrini *et al* [39], but remained unexplained. Possibly the photoconductivity signal did not arise from an ordinary Sm^{2+} site. Fuller and McClure [40] reported photoconductivity thresholds for Eu^{2+} and Sm^{2+} in SrF_2. They are indicted by arrows 1 and 2 in figure 10. The threshold for Eu^{2+} is larger than the threshold from [13] and, as for the threshold for Sm^{2+}, the arrows end significantly above the bottom of the conduction band. It was suggested that nearby interstitial fluorine ions lead to smaller ionization energies. This again illustrates that one should be very careful in the interpretation of photoconductivity data and that the defect structure can be very important.

5. Summary and conclusions

The anomalous emission in Eu^{2+}- and Yb^{2+}-doped compounds has been studied. First, cases of anomalous emission were identified from the literature, and data have been collected. Clear trends concerning the probability for anomalous emission to occur were found: (1) the probability of anomalous emission increases with increasing size of the cation site; (2) the probability increases when the binding strength of oxygen decreases; (3) the probability decreases with increasing size of the anions; (4) the probability increases with decreasing size of the lanthanide ion; (5) normal df emission is never observed for divalent lanthanides on trivalent cation sites and always observed for divalent lanthanides on monovalent cation sites.

The trends have been explained qualitatively. The change in Madelung potential due to lattice relaxation around the lanthanide ion, the Coulomb interaction between the 5d electron

and the lanthanide ion, and the isotropic exchange interaction between the 5d electron spin and the total spin of the $4f^{n-1}$ electrons create a variation of the 5d electron ionization energy $I_d(n, 2+, A)$. This variation combined with the known systematic variation in fd transition energies allows one to derive the energy levels of the divalent lanthanides relative to the conduction and valence band states. The lowest 5d level of Yb^{2+} on a Ca^{2+} or Sr^{2+} site is always very close to the conduction band. On a Ba^{2+} site the lowest 5d level is usually located inside the conduction band. That of the other lanthanides can be found within 1.24 eV from the bottom of the conduction band.

At this moment it is not yet clear whether the variation in $I_d(n, 2+, A)$ with n suggested for CaF_2, SrF_2, and BaF_2 remains the same in other compounds. To verify this, detailed knowledge of either $I_d(n, 2+, A)$ or $I_f(n, 2+, A)$ for different lanthanides in a wide variety of different compounds is needed. Such information can be obtained with photoconductivity or ultra-violet photoelectron spectroscopy (UPS) techniques. Studies on the absence or presence of vibrational structure in fd excitation spectra also provide information of $I_d(n, 2+, A)$. Once the 5d state is populated, the 5d electron can be excited to the conduction band by means of photons or by means of phonons. Therefore excited state absorption and thermal quenching of df emission also provide information on the location of the 5d level [66, 67]. Last but not least, the energy needed for charge transfer from the valence band to the trivalent lanthanide provides information on the location of the $4f^n$ ground state of the divalent lanthanide relative to the valence band [68–70].

Each of the above techniques have been applied to determine the location of impurity levels. However, they all have systematic errors and are often applied to a very limited number of lanthanides in a very limited number of compounds. A study comprising many different lanthanides in many different compounds with many different techniques is needed. Only then can a consistent energy level scheme be constructed that removes the systematic errors implicit to each technique. The anomalous luminescence of the divalent lanthanides treated in this work can be seen as a first step in that effort.

References

[1] Dorenbos P 2000 *J. Lumin.* **91** 91
[2] Dorenbos P 2003 *J. Phys.: Condens. Matter* **15** 575
[3] Henderson B and Imbush G F 1989 *Optical Spectroscopy of Inorganic Solids* (Oxford: Clarendon)
[4] Kaplyanskii A A and Feofilov P P 1962 *Opt. Spectrosc.* **13** 129
[5] Reut E G 1976 *Opt. Spectrosk.* **40** 55
[6] Kaplyanskii A A, Medvedev V N and Smolyanskii P L 1976 *Opt. Spectrosk.* **41** 615
[7] Kaplyanskii A A, Medvedev V N and Smolyanskii P L 1977 *Opt. Spectrosk.* **42** 74
[8] Reut E G 1978 *Opt. Spectrosk.* **45** 290
[9] Pedrini C, McClure D S and Anderson C H 1979 *J. Chem. Phys.* **70** 4959
[10] Pedrini C, Pagost P O, Madej C and McClure D S 1981 *J. Physique* **42** 323
[11] McClure D S and Pedrini C 1985 *Phys. Rev.* B **32** 8465
[12] Moine B, Courtois B and Pedrini C 1989 *J. Physique* **50** 2105
[13] Moine M, Pedrini C and Courtois B 1991 *J. Lumin.* **50** 31
[14] Lizzo S, Meijerink A and Blasse G 1994 *J. Lumin.* **59** 185
[15] Lizzo S, Meijerink A, Dirksen G J and Blasse G 1995 *J. Phys. Chem. Solids* **7** 959
[16] Lizzo S, Meijerink A, Dirksen G J and Blasse G 1995 *J. Lumin.* **63** 223
[17] Lizzo S, Klein Nagelvoort E P, Erens R, Meijerink A and Blasse G 1997 *J. Phys. Chem. Solids* **58** 963
[18] Poort S H M, Blokpoel W P and Blasse G 1995 *Chem. Mater.* **7** 1547
[19] Poort S H M and Blasse G 1997 *J. Lumin.* **72–74** 247
[20] Jagannathan R and Kutty T R N 1997 *J. Lumin.* **71** 115
[21] Lyu Li-Ji and Hamilton D S 1991 *J. Lumin.* **48/49** 251
[22] Dorenbos P, Bos A J J and van Eijk C W E 2002 *J. Phys.: Condens. Matter* **14** L99

[23] Dorenbos P, van Eijk C W E, Bos A J J and Melcher C L 1994 *J. Lumin.* **60/61** 979
[24] Hamilton D S, Gayen S K, Pogatshnik G J and Shen R D 1989 *Phys. Rev.* B **39** 8807
[25] Dorenbos P 2003 *J. Lumin.* at press
[26] Kobayasi T, Mroczkowski S, Owen J F and Brixner L H 1980 *J. Lumin.* **21** 247
[27] Dorenbos P 2000 *J. Lumin.* **91** 155
[28] Sommerdijk J L and Bril A 1976 *J. Lumin.* **11** 363
[29] Schipper W J, Piet J J, de Jager H J and Blasse G 1994 *Mater. Res. Bull.* **29** 23
[30] Meijerink A 1993 *J. Lumin.* **55** 125
[31] Nikl M, Mihokova E, Malikova Z, Vedda A, Martini M, Shimamura K and Fukuda T 2002 *Phys. Rev.* B **66** 184101
[32] Alcala R, Sardar D K and Sibley W A 1982 *J. Lumin.* **27** 273
[33] Tomiki T and Miyata T 1969 *J. Phys. Soc. Japan* **27** 658
[34] Sugar J and Reader J 1973 *J. Chem. Phys.* **59** 2083
[35] Sekiya M, Narita K and Tatewaki H 2000 *Phys. Rev.* A **63** 012503
[36] Shannon R D 1976 *Acta Crystallogr.* **32** 751
[37] Yanase A 1977 *J. Phys. Soc. Japan* **42** 1680
[38] Payne S A, Chase L L, Krupke W F and Boatner L A 1988 *J. Chem. Phys.* **88** 6751
[39] Pedrini C, Rogemond F and McClure D S 1986 *J. Appl. Phys.* **59** 1196
[40] Fuller R L and McClure D S 1991 *Phys. Rev.* B **43** 27
[41] Dorenbos P 2002 *Phys. Rev.* B **65** 235110
[42] Bonch-Bruevich V A and Ovsyankin V V 1975 *Sov. Phys.–Solid State* **17** 587
[43] Fuller R L and McClure D S 1987 *J. Lumin.* **38** 193
[44] Kiss Z J 1962 *Phys. Rev.* **127** 718
[45] Henke M, Persson J and Kück S 2000 *J. Lumin.* **87–89** 1049
[46] Henderson E W and Meehan J P 1974 *J. Lumin.* **8** 415
[47] Kück S, Henke M and Rademaker K 2001 *Laser Phys.* **11** 116
[48] Loh E 1969 *Phys. Rev.* **184** 348
[49] Zapasski V S and Feofilov P P 1976 *Opt. Spectrosk.* **41** 620
[50] Schipper W J and Blasse G 1991 *J. Solid State Chem.* **94** 418
[51] An C P, Dierolf V and Luty F 2000 *Phys. Rev.* B **61** 6565
[52] Bland S W and Smith M J A 1985 *J. Phys. C: Solid State Phys.* **18** 1525
[53] Muller M, Fabris J L, Hernandes A C and Siu Li M 1993 *Phys. Status Solidi* b **180** K93
[54] Pologrudov V V and Ibragim Z D 1999 *Phys. Solid State* **41** 1617
[55] Tsuboi T, Witzke H and McClure D S 1981 *J. Lumin.* **24/25** 305
[56] Kaplyanskii A A, Medvedev V N and Smolyanskii P L 1976 *Opt. Spectrosk.* **40** 301
[57] Wagner M and Bron W E 1965 *Phys. Rev.* **139** A223
[58] Palilla F C, O'Reilly B E and Abbruscato V J 1970 *J. Electrochem. Soc.: Solid State Sci.* **117** 87
[59] Dotsenko V P, Berezovskaya I V, Pyrogenko P V, Efrushina N P, Rodnyi P A and van Eijk C W E 2002 *J. Solid State Chem.* **166** 271
[60] Blasse G, Dirksen G J and Meijerink A 1990 *Chem. Phys. Lett.* **167** 41
[61] Pei Zhiwu, Su Qiang and Zhang Jiyu 1993 *J. Alloys Compounds* **198** 51
[62] Gaft M L and Gorobets B S 1979 *J. Appl. Spectrosk.* **31** 1488
[63] Gorobets B S, Portnov A M and Rogozhin A A 1995 *Radiat. Meas.* **24** 485
[64] Donohue P C and Hanlon J E 1974 *J. Electrochem. Soc.: Solid State Sci. Technol.* **121** 137
[65] Lehmann W 1972 *J. Lumin.* **5** 87
[66] Merkle L D and Bandyopadhyay P K 1989 *Phys. Rev.* B **39** 6939
[67] Merkle L D 1990 *Phys. Rev.* B **42** 3783
[68] Nakazawa E 2002 *J. Lumin.* **100** 89
[69] Gerard I, Krupa J C, Simoni E and Martin P 1994 *J. Alloys Compounds* **207/208** 120
[70] Ionova G, Krupa J C, Gerard I and Guillaumont R 1995 *New J. Chem.* **19** 677